



ISSN (PRINT) : 2320 -1967  
ISSN (ONLINE) : 2320 -1975



## ORIGINAL ARTICLE

CHEMXPRESS 9(1), 030-045, (2016)

# Effect of sonication irradiation on degradation of refinery petroleum wastewater using the prepared cationic silyl polymeric surfactant

Z.Abdeen<sup>1\*</sup>, Abdelfattah M.Badawi<sup>1</sup>, Ahmed I.Adawi<sup>1</sup>, Akram M.Eldidamony<sup>2</sup>, Abd El-Shafey I.Ahmed<sup>2</sup>, Eslam Hafez<sup>1</sup>

<sup>1</sup>Petrochemical Department, Egyptian Petroleum Research Institute, Nasr City, Cairo, (EGYPT)

<sup>2</sup>Chemistry Department, Faculty of Science, Zagazig University, (EGYPT)

E-mail: ziziabdeen@yahoo.com

Received : 29<sup>th</sup> November, 2014 ; Revised : 14<sup>th</sup> March, 2015 ; Accepted : 17<sup>th</sup> March, 2015

**Abstract :** The influence of ultrasonic and Fenton reagent combination on the efficiencies of each metal complex of quaternized poly (4-vinyl pyridine) (P4-VP), and its nanocomposites (CS) in degradation of refinery petroleum wastewater, was studied. P4-VP was quaternized by chloro tri methyl silane then complexed with ferric chloride, that reacted with nano zero valent iron given CS. It was resulted an

enhancement on oil degradation % using this combination system, was 85%, making this method may be used in water treatment.

© Global Scientific Inc.

**Keywords :** Poly (4-vinyl pyridine); Sonication; Quaternization; Complex; H<sub>2</sub>O<sub>2</sub>; Fenton.

## INTRODUCTION

In the petroleum industry, oily water occurs in the stages of production, transportation and refining, as well as during the use of derivatives. However, the production phase is the largest source of this pollution. The removal of oil pollutants are often performed by physical or chemical processes. These methods are commonly expensive with the potential of producing by-product pollutants<sup>[1]</sup>. Advanced oxidation processes are used for removing organic hydrocarbons. Fenton's method has more advantages comparing to other methods since it is

cheaper, reduced reaction time and energy consumption, non-toxic nature of the compounds, and operation and control simplicity<sup>[2]</sup>. The basis of the Fenton method is the decomposition of H<sub>2</sub>O<sub>2</sub> and the production of hydroxyl radicals in the presence of Fe<sup>3+</sup> ions as a catalyst<sup>[3-4]</sup>. Studies have shown that produced hydroxyl radicals are capable of decomposing and degrading organic contaminants such as petroleum hydrocarbons<sup>[5-6]</sup>. Ultrasonic irradiation generates benefits in heterogeneous catalytic systems by decreasing mass transfer limitations and fragmentation of catalyst in small particles that provide a higher surface area<sup>[7-10]</sup>. Moreover, the additional gen-

eration of free radical species in ultrasound systems should enhance the overall catalytic performance<sup>[10-11]</sup>.

Liang et al.<sup>[12]</sup>, observed that the combination of ultrasonic irradiation with the addition of iron powder results in a significant enhancement to the 4-chlorophenol degradation rate when hydrogen peroxide is present. Similar results have been reported by<sup>[13]</sup>. Therefore, the combination of ultrasonic treatment and Fenton reagent represents a promising new technique in the field of environmental engineering. Neppolian et al.,<sup>[14]</sup> reported that a heterogeneous Fenton system coupled with ultrasound using a heterogeneous iron catalyst (Fe-OOH) appears to be a promising method, showing relatively high degradation rates of para-chlorobenzoic acid compared to ultrasound alone or silent fenton mode. Also, Nanoscale iron particles represent a new generation of environmental remediation technologies that could provide cost-effective solutions to some of the most challenging environmental cleanup problems<sup>[15]</sup>. Nanoparticles show a higher catalytic activity because of their small size (10-100nm) and their large specific area<sup>[16]</sup>. As an alternative to surfactants, the controlled coating of nano scaled zero iron valent (nZVI) with high molecular weight polymers may be considered an irreversible process and therefore provides a more appropriate method for increasing the hydraulic mobility of nZVI in subsurface systems. Working in the same way as surfactants to promote colloidal stability (steric hindrances) the polymer is physically or chemically grafted to the nanoparticle surface<sup>[17]</sup>. An additional benefit is that the polymer coatings may also act as an energy source to stimulate catalytic activity, which may aid contaminant removal. Water-soluble cationic polymers are a class of polyelectrolyte that useful in many applications, including sludge dewatering<sup>[18]</sup>, the design of new membranes<sup>[19]</sup>, etc. They derive their unique properties from the density and distribution of positive charges along the macromolecular backbone. Chain conformation and solubility of such flocculants depend on the extent of ionization and interaction with water. Cationic functional groups can strongly interact with suspended, negatively charged particles or oil droplets. Water-

soluble polymers containing cationic charge can be divided into three categories: ammonium (including amines), sulfonium and phosphonium quaternaries Poly (2-Vinyl Pyridine) and Poly (4-Vinyl Pyridine). The polymers are quaternized with alkyl derivatives to form strong polyelectrolytes in solution. An alternative choice to attain quaternary ammonium polymers may be the quaternization of polyvinyl pyridines. Preparation of vinyl pyridinium monomers is almost impossible due to their spontaneous polymerization yielding pyridinium moieties in the main chain<sup>[20]</sup>. In addition, post quaternization of the P (4-VP) does not proceed with quantitative conversions. The most common is 65–70% of quaternization with alkyl halides that has been credited to the neighboring group effect<sup>[21]</sup>. The most favorable reagent to attain high quaternization yields, up to 95%, is the methyl iodide (iodomethane). As much as, it is known a quantitative quaternization of P (4-VP), has not been reported no further. In this work, we describe a simple procedure for quaternization of P (4-VP) with chloro tri methyl silane that has not been reported, and then complexes the quaternized polymer prepared (Q) with ferric chloride. As well, the metal nanocomposites (CS) of the Q with nZVI were prepared and their surface properties were studied. The effect of pH solution, concentration of C & CS and the time on oil degradation process was studied. Ultrasonic irradiation with/ without heterogeneous catalytic systems reactions, modified Fenton reactions were applied to examine them in degradation of oil contaminated in wastewater.

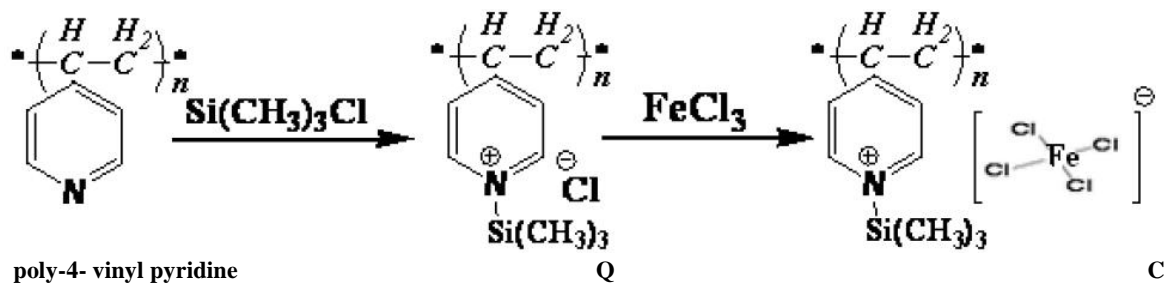
## EXPERIMENTAL SECTION

### Materials

poly-4-vinyl pyridine(60,000), chlorotrimethylsilane, Zinc chloride anhydrous, Sodium borohydride Ferric chloride, Paraffin oil, Hydrogen peroxide and all others chemicals were purchased from Aldrich company. We obtained the commercial emulsifier from Egyptian Petroleum Research Institute and the Crude oil from Egyptian petroleum company.

### Quaternization of poly-4- vinyl pyridine (60,000) by chlorotrimethylsilane

## ORIGINAL ARTICLE



Scheme 1 : Synthesis of quaternary salt metal complex

poly-4- vinyl pyridine (5.25 g, 0.05 mole repeating unit) was dissolved in 25 ml DMF and 75.0 mmol. of chlorotrimethylsilane, the solution was stirred at room temperature. The mixture became a pale yellow and a white precipitate of quaternary salt (N-trimethylsilane poly-4-vinyl pyridinium chloride) Q was formed at once, as shown in the scheme 1. At the end of reaction, the mixture was filtered and washed with acetone then ether. Vacuum dried products were stored in tightly closed dark as shown in the scheme 1.

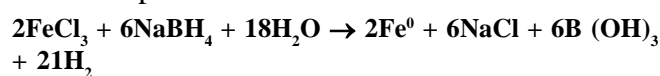
#### Synthesis of quaternary salt metal complex

The prepared quaternary salt (5 g) was dissolved in 100 ml methanol and 5g of ferric chloride was dissolve in 20 ml methanol then pour them in flask 250 ml and reflux for 4 hours. The mixture became a red and a brown precipitate of quaternary salt complex was formed as shown in the scheme 1. At the end of reaction, the mixture was filtered and washed with methanol.

#### Preparation of the nano scaled zero valent iron (nZVI)

For the synthesis of NZVI, a 0.5406 g  $\text{FeCl}_3 \cdot 6\text{H}_2\text{O}$  was dissolved in a 4/1 (v/v) ethanol/deionized water mixture with well stirring. On the other hand, 0.1 M sodium borohydride solution was prepared by dissolving a 0.3783 g  $\text{NaBH}_4$  in 100 ml of deionized water; since for better growth of iron nanoparticles excess borohydride is needed. The borohydride solution is added drop by drop into iron chloride solution with vigorous hand stirring. After the first drop of sodium borohydride solution, black solid particles appeared and the remaining sodium borohydride is added completely to accelerate the reduction reaction and the mixture was left for another 10 minutes of stirring. The vacuum filtration

technique was used to separate the black iron nanoparticles from the liquid phase and then, they were washed three times with absolute ethanol to remove all of the water and prevent the rapid oxidation of zero valent iron nanoparticles. The synthesized nanoparticles were finally dried in oven and storage in a thin layer of ethanol was to preserve the nano iron particles from oxidation.



#### Synthesis of nano scaled zero valent iron (nZVI) self-assembled and stabilized by quaternary salt

The prepared quaternary salt (5 g) was dissolved in 100 ml ethanol. A 0.5g of prepared zero valent iron nanoparticles were sonicated in 50 ml ethanol and added drop wise to the solution of quaternary salt with stirring. The nZVI self-assembled by quaternary salt was obtained at changed the solution color to pale brown turbidity with continued stirring for 4h. Then the solution centrifuged at 3000 rpm for 10 min and the supernatant was washed with ethanol.

#### Synthetic oil-water emulsion

The concentrated stock oil-water emulsion (10g/L) was prepared using tap water containing 1% NaCl and mixing process at a rate of 2.5 ml/min with a blender speed 60 rpm. A 5% of the appropriate emulsifier was used with mixing and gentle heating it for 2.5-3 hrs, to obtain a homogenous solution.

#### Surface tension measurements

The synthesized cationic complex solution were used with the concentration range from  $10^{-5}$  to  $10^{-1}$  molar at 25 °C. The solutions were poured into a clean Teflon cup with a mean diameter of 40 mm and were left for 2 hours to allow the stabilization

and complete adsorption at the solution surface and the apparent surface tension ( $\gamma$ ) values were measured<sup>[22]</sup>.

### Effectiveness ( $\pi_{cmc}$ )

The effectiveness is defined as the difference between the surface tension of the bi-distilled water ( $\gamma_o$ ) and that of the surfactant solution ( $\gamma_{cmc}$ ) at the critical micelle concentrations as follows:

$$\pi_{cmc} = \gamma_o - \gamma_{cmc}$$

### Efficiency (PC20)

Efficiency (PC20) is determined by the concentration (mol/liter) of the surfactant solutions capable to suppress the surface tension by 20 dyne/cm.

### Emulsion stability

Emulsion stability was measured by vigorously stirring a mixture of 10 mL (0.1%) of the synthesized quaternary polymeric salt solutions and 10 mL of paraffin oil at 25°C<sup>[23]</sup>. Emulsifying power (emulsion stability) of the surfactant solutions were expressed as the time required for separation of 9 mL of pure surfactant solution.

### Treatment of oily wastewater sample and estimated of the remaining crude oil by a gravimetric method

One hundred grams of oily wastewater and different amount of modified complexes were mixed together at room temperature and stirring for different times. The oil sample was extracted from oily wastewater by carbon tetrachloride in separating funnel and the solvent was removed by using a rotary evaporator. The percentage of the degradation (the remaining oil) was calculated.

### Structural analysis

The molecular structure of the samples was obtained, by using the IR transmission spectroscopic. The investigation was carried out at room temperature on FT-IR, JASCO, Nicolet IS-10(made in Japan) spectrometer using KBr disc method with a spectral resolution of 4 cm<sup>-1</sup> over the wave number range of 400-4000 cm<sup>-1</sup>. X-ray diffraction (XRD) studies were performed to identify the crystalline species present. XRD measurements were carried

out at room temperature on a Philips model PW 1050 diffractometer, using CuK (wavelength = 1.54 Å) radiation source filtered by a graphic monochromatic operating at capacity of 30 kV and a current of 40 mA.

The surface morphology of samples was examined from micrographs taken with a scanning electron microscopy (SEM, TOPCON ABT150S, and Japan). Prior to observation, samples were mounted on metal grids and coated with gold under vacuum before observation. Also, the size of samples was determined by transmission electron microscopy (TEM, Model JEM-200CX, JEOL and Japan). A few quantities of sample were dispersed in 10 ml ethanol and sonicated for 30min. A few drops of the resulting suspension were placed on a covered copper grid. The Raman measurement was carried out as follows: quaternary salt and its complex by Dispersive Raman spectroscopy at laser 785 nm and laser power 0.10 MW, Senterra, Bruker optics, Germany. The atomic absorption spectroscopy is an accurate method of quantitative analysis for many elements like iron. Flame atomic absorption spectrometer/ ZEE nit 700p/ Analytikjena.Co/ Germany. The surface tension was measured by using the Tensiometer K6 Krüss, Germany.

The pore size and surface area of the samples was determined with Brunauer-Emmett-Teller (BET) surface area analyzer. The sample was placed in sample cells, which were then heated up to 348 K for 3 h and cooled down to room temperature to remove moisture from the sample before the BET analysis. The BET pore size and surface area was determined with N<sub>2</sub> adsorption. The Pore size distribution (PSD) was calculated from the analysis of the desorption branch of the adsorption-desorption isotherms using the Barrett-Joyner-Halenda (BJH) algorithm. The *t*-plot method was used for analyzing microporosity in the sample.

We measure the absorption of quaternary salt and its complex by UV/V spectrophotometer (JASCO, V570, and USA). The concentration of chloride in the quaternary salts was determined by ion selective electrode for chloride TIM 900 titration manager (Ridionteer analytical, Copenhagen, Denmark).

# ORIGINAL ARTICLE

## RESULTS AND DISCUSSION

### Structural characterizations

Figure 1 showing the IR spectra of [P (4-VP)], Q, C and CS, it was revealed that the several absorption bands at 3063- 3023  $\text{cm}^{-1}$  corresponding to C-H stretching in aromatic, and at 2926- 2757  $\text{cm}^{-1}$  in aliphatic. The bands appeared at 2069- 1938, 1632- 1597 and 1607-1550  $\text{cm}^{-1}$  are due to overtone, C=N group and C=C group respectively. A shift to higher frequency of C=C was occurred because of quaternization in spectra of Q, C and CS. As well, the bending bands of  $\text{CH}_2$  around 1457- 1415  $\text{cm}^{-1}$  and at 1219- 1202  $\text{cm}^{-1}$  of C-N while the absorption

bands of aromatic ring bending are at 814-746  $\text{cm}^{-1}$ , Figure 1. Also, the absorption bands at 1256- 1248  $\text{cm}^{-1}$  and 667  $\text{cm}^{-1}$  corresponding to Si-C and Fe-Cl, respectively, Figure 1. The Raman spectra of quaternary Q and its ferric chloride modification complex C are shown in Figure 2. There are five main absorption bands for the quaternary Q at 1206, 1006, 653 and 77  $\text{cm}^{-1}$ , which were assigned to the vibrations of the quaternary cation. Also, the Raman spectrum of complex C has these bands with a small shift in position and difference in band area. The Raman spectrum of complex C shows a strong absorption bands at 332 related to the symmetric Fe-Cl. The UV spectra of quaternary Q and its complex C ap-

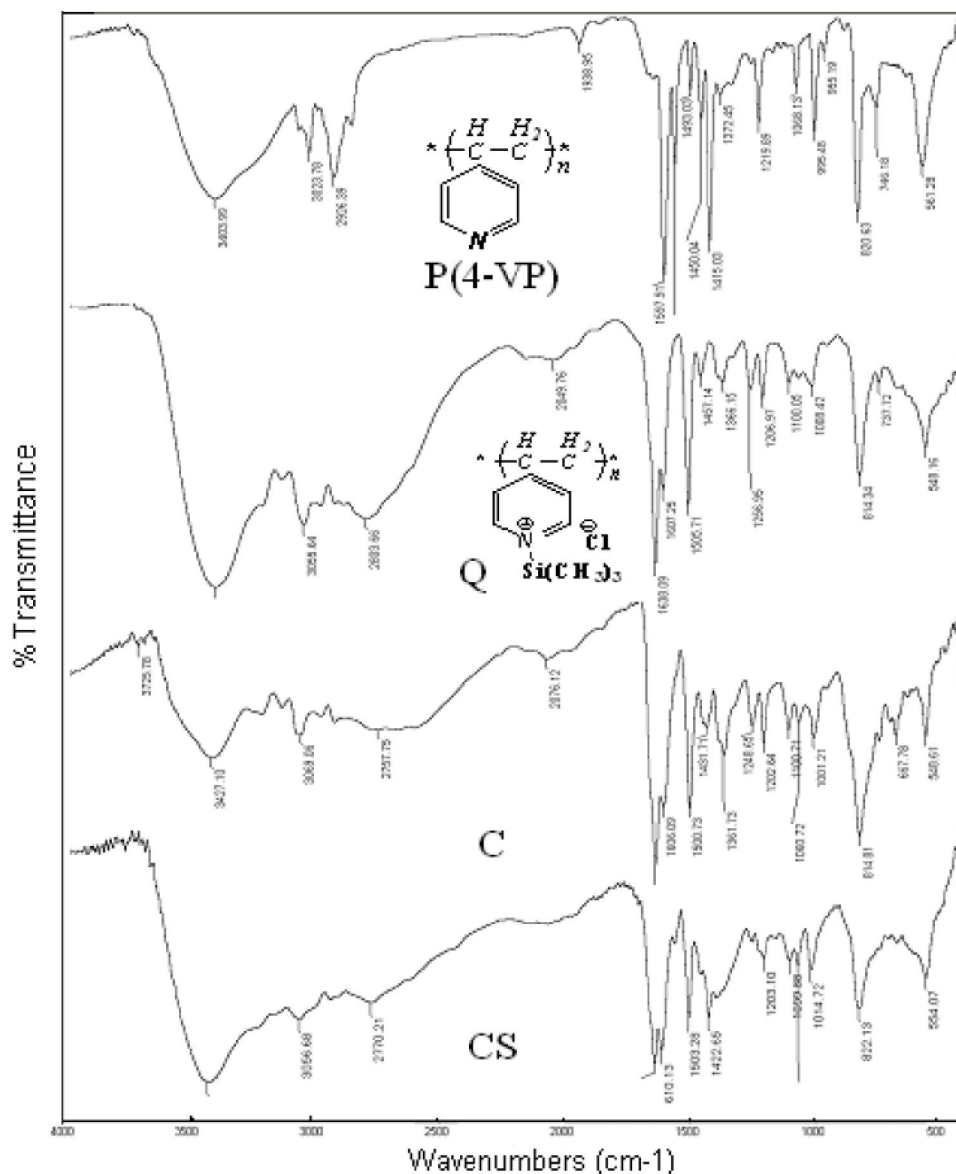


Figure 1 : Infrared spectroscopy for [P (4-VP)], Q, C and nanocomposite CS

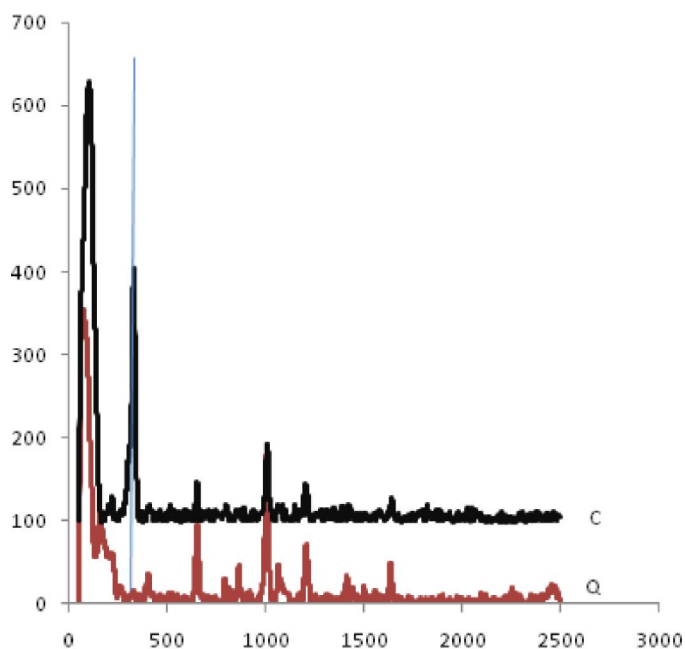


Figure 2 : Raman spectroscopy for quaternary Q &amp; complex C

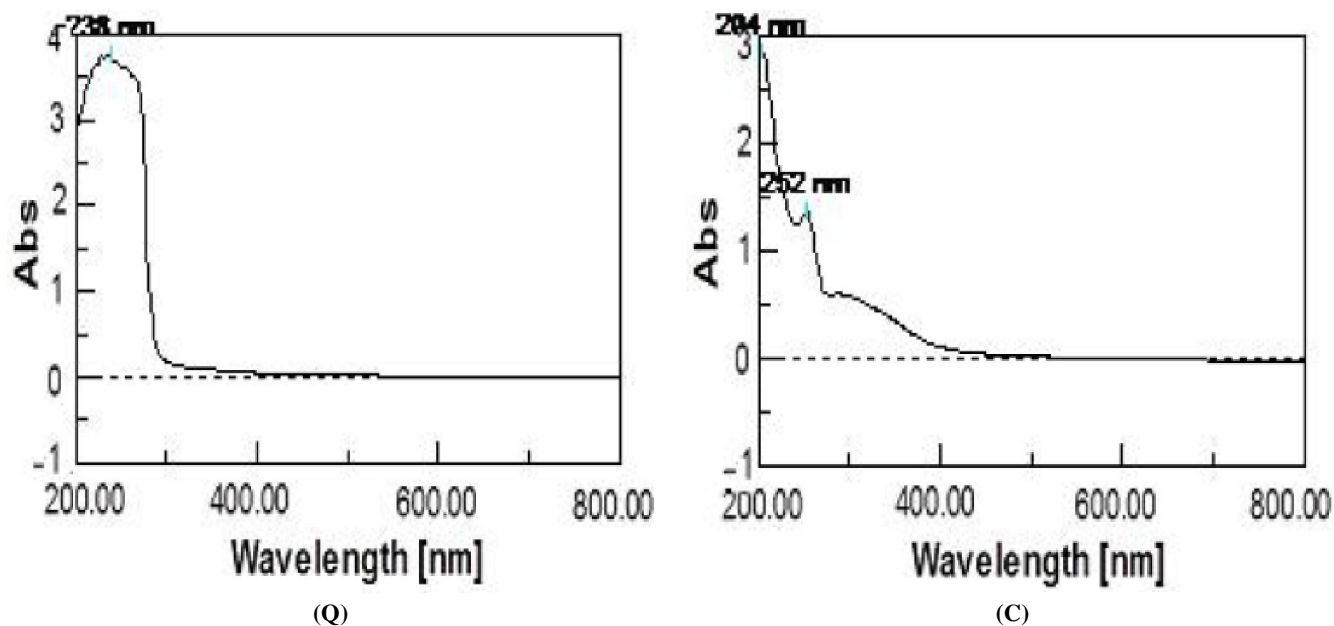


Figure 3 : UV spectra of quaternary Q &amp; complex C

pear in Figure 3, where, there is a main absorption band for the quaternary Q at 238 nm, but this absorption band appears strong at 252 in UV spectrum of complex C with a small shift in position and a difference in band area assigned to tetrachloroferrate.

The Figure 4 shows the transmission electron microscopy image of iron nanoparticles, which have spheres having diameters of around 100 nm. The metallic iron and iron oxide phases can be distinguished from the corresponding color contrast in

TEM images, where, the lighter regions are mainly on the surface of the particle and the dark regions are concentrated in the center of the particle. It is obvious in Figure 4 of the TEM micrograph of the quaternized salt Fe nanocomposite CS that the core is formed of metallic iron and the surface (shell) is formed of iron oxides. The iron nanoparticles are well-dispersed in the quaternized salt matrix and aggregation is minimal. After the formation of the nanocomposites the iron particles (dark shaded) are

# ORIGINAL ARTICLE

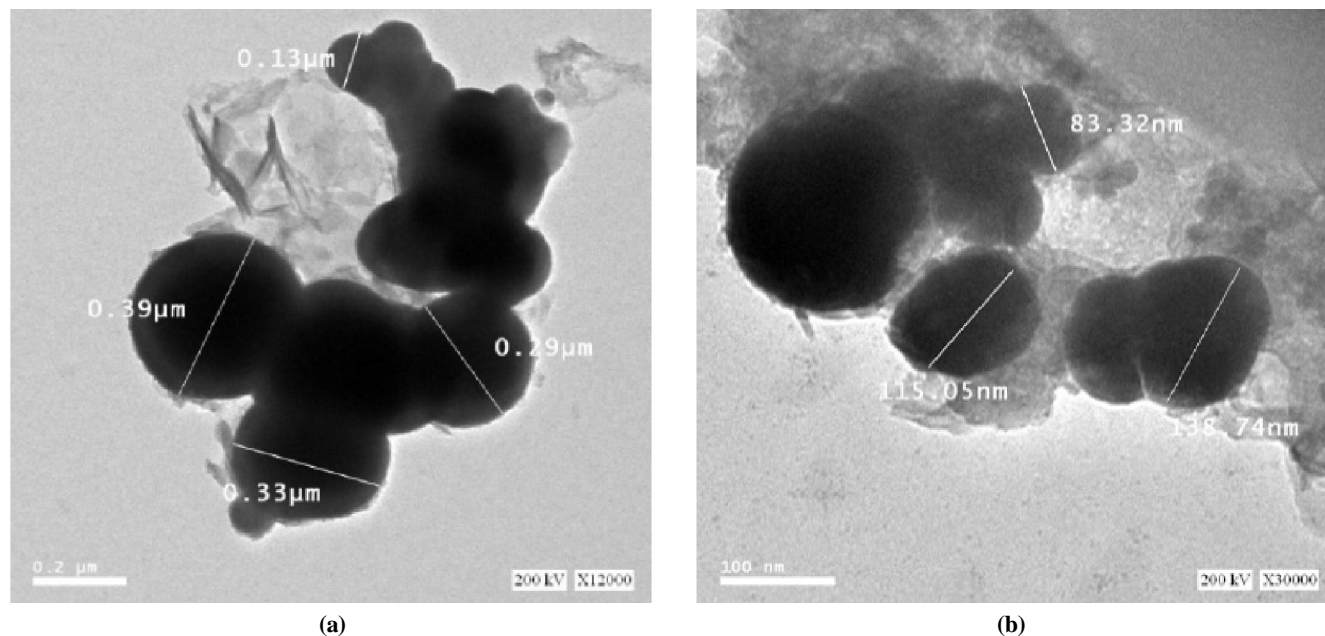


**Figure 4 :** TEM images of iron nanoparticles (nZVI) (a) and the colloidal iron nanoparticles (FeNPs) with Q self-assembled (b)

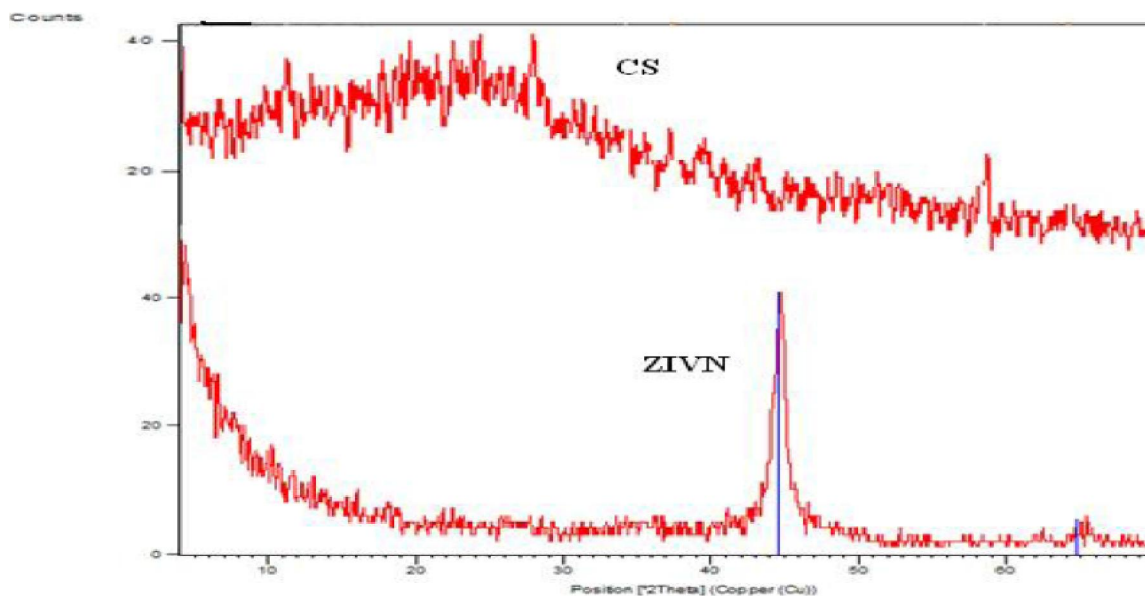


**Figure 5 :** X-Ray Diffraction of zero iron valent nanoparticles (ZIVN) and nanocomposite CS

found to be entrapped into quaternized salt (light shaded) chains indicating that the iron particles are simply interchelated with the polymer.

The XRD pattern of nZVI powder samples under ambient conditions is shown Figure 5. The broad peak reveals the existence of an amorphous phase of iron and the characteristic broad peak at  $2\theta$  of  $45^\circ$  indicates that the zero valent iron is predominantly present in the sample<sup>[24]</sup>. This peak was disappeared in XRD pattern of the nanocomposite CS

referring to the presence of the quaternary salt in the iron that, decrease the crystallinity of the zero valent iron and intercalated in it, where these results is agreed with that of TEM.

The BET surface area value,  $34.75 \text{ m}^2/\text{g}$  of nZVI is obtained from Figure 6. In comparison with some of the BET surface area values reported in literature are  $14.5 \text{ m}^2/\text{g}$ ,<sup>[25]</sup>  $33.5 \text{ m}^2/\text{g}$  and  $36.5 \text{ m}^2/\text{g}$ <sup>[26]</sup>. The commercially available Fe powder ( $<10 \mu\text{m}$ ) has a specific surface area of just  $0.9 \text{ m}^2/\text{g}$ <sup>[27]</sup> where,

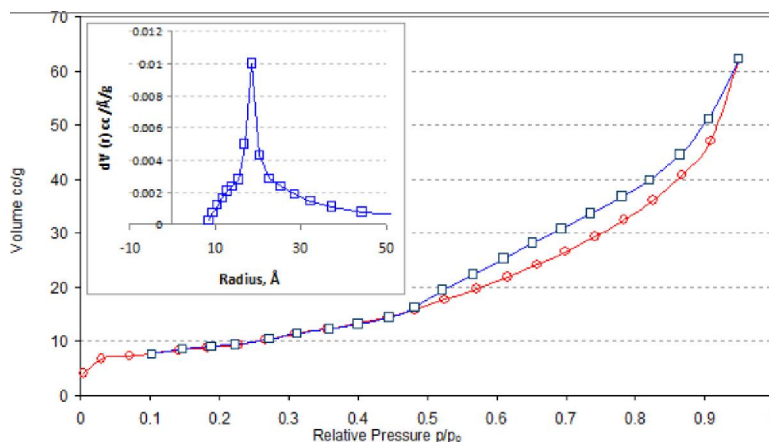


Figure 6 : BET adsorption-desorption isotherms of Fe nanoparticles with surface area of  $\approx 35\text{m}^2/\text{g}$ .

TABLE 1 : Surface properties for nZVI

Specific Surface Area, $\text{m}^2/\text{g}$	Total Pore Volume, $\text{cc}/\text{g}$	pore radius, $\text{\AA}$
34.75	0.90603	18.596 (1.86 nm)

the increase in specific surface area means an increase in the total amount of iron on the surfaces. Therefore, it is evident that nanoscaled zero valent irons (nZVI) (50-100 nm) with good properties are synthesized in ethanol medium by sodium borohydride reduction method under atmospheric condition. The porosity is available from the pore volume distribution curve as shown in Figure 6, it constructed by plotting  $DV/p/Dr$  against the pore radius.

Where, the maxima of the pore radius and pore diameter distribution curves are located at range of 1.86 and 3.7 nm, respectively, TABLE 1.

The morphology of iron nano particle was confirmed by scanning electron microscope (SEM), Figure 7. It appears that the SEM image of Fe includes the small particles and the surface of quaternary Q sample is smooth, but is winding and full of pores with respect to nanocomposite CS, that has fairly well-dispersed Fe nanoparticles in its nanocomposite network. The concentration of chloride in a solution contain 1000 ppm of Q is 93 ppm and this indicates that the quaternization occur by 40 % of poly-4- vinyl pyridine. Also, the concentration of iron in a solution contains 1000 ppm of complex C was measured by atomic absorption spectroscopy. It is 112 ppm confirmed that every part of quaternized site make tetrachloro ferrate and the quaternization occur by 40 % of poly-4- vinyl pyridine.

### Surface active properties of the quaternary ammonium salts Q and its complex C

The Figure 8 shows the surface tension concentration profile of the synthesized cationic polymeric surfactant Q and its complex C in their solutions at  $25^\circ\text{C}$ , has two characteristic regions. In the first region, the surface tension is continually decreases by increasing the surfactant concentration due to accumulate of the surfactant molecules in the air/water interface. The surface tension change in the second region is almost stable by increasing the surfactant concentration, which indicates no further adsorption is occurred at the interface. The intercept of the two regions gives the concentration at which the micelles are formed (the critical micelle concentration, CMC)<sup>[28]</sup>. As shown in TABLE 2, the lower CMC value is appeared to the quaternized Q with respect to that of C.

The values of  $\Gamma_{\text{cmc}}$  of the synthesized cationic surfactant and its complex C were listed in TABLE 2. It is clear that the increasing of the hydrophobicity surfactant molecule leads to increase the effectiveness at constant temperature as in surfactant Q (Quraishi and Shukla, 2009). Another important factor that determines the surface activity of the surfactant molecules at the interface is the maximum surface excess,  $\Gamma_{\text{max}}$ , which can be evaluated by applying Gibb's equation as given in the following equation<sup>[29]</sup>:

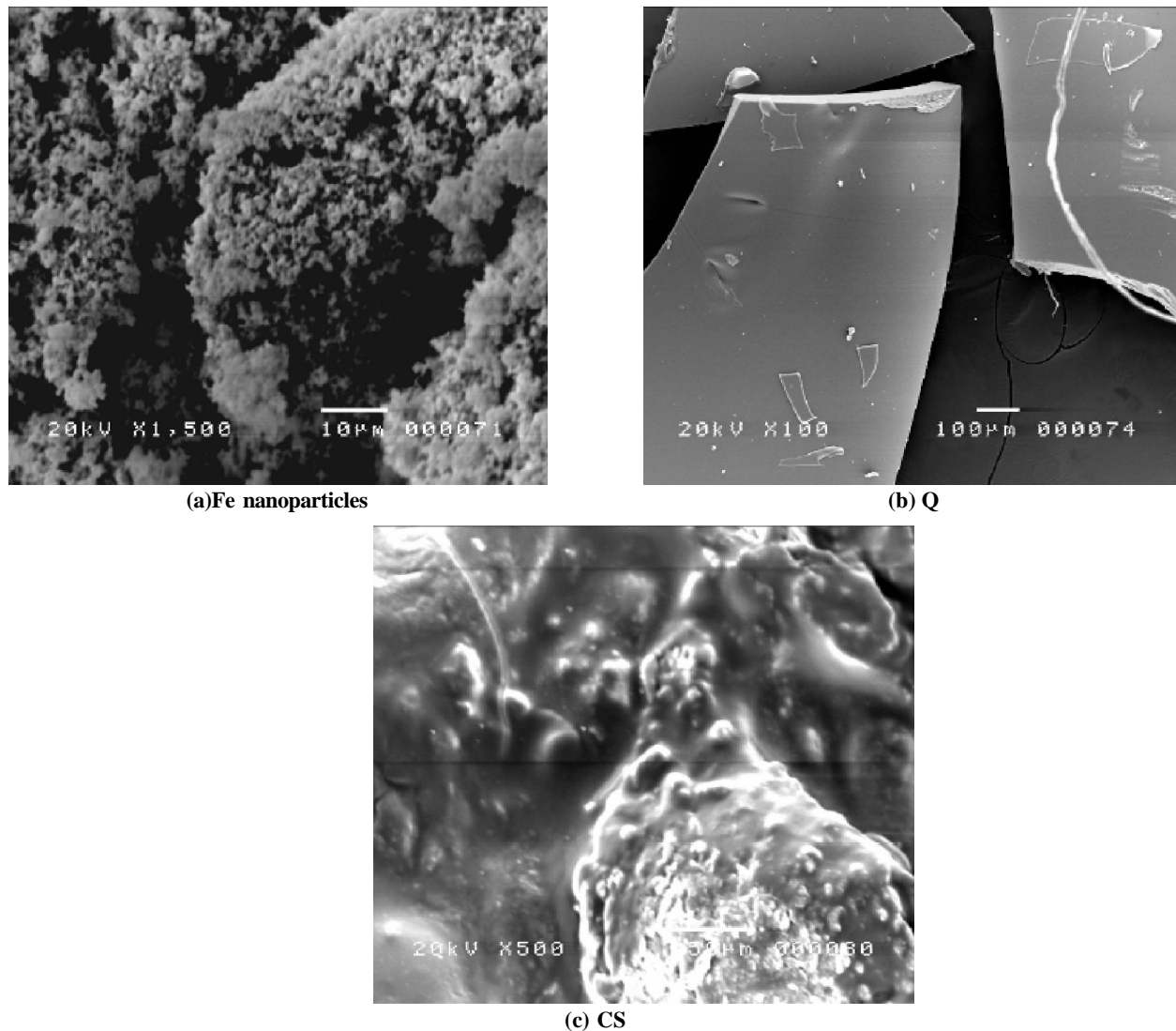


Figure 7 : The SEM images of Fe nanoparticles (a), Q (b) and CS (c)

$$\Gamma_{\max} = - (1 / 2.303 nRT) (\delta \gamma / \delta \log c)_{\text{T}}$$

where,  $\gamma$  is the equilibrium surface tension in dyne/cm,  $R$  is the gas constant ( $8.314 \text{ mol}^{-1} \text{ K}^{-1}$ ),  $T$  is the absolute temperature,  $C$  is the surfactant concentration, and  $(\delta \gamma / \delta \log c)$  is the surface pressure. The value of  $n$  expresses the number of solute species and equal to 2 for conventional ionic surfactants. In general the maximum surface excess at the interface are increased by increasing the hydrophobic chain length and this can be attributed to increasing of the hydrophobicity of the molecules that increases the tendency of adsorption of surfactant molecules, as a consequence,  $\Gamma_{\max}$  increased indicating higher surface concentration and increasing number of surfactant molecules at the surface. The minimum surface area values occupied by the synthesized cationic

surfactants at the interface,  $A_{\min}$ , ( $\text{nm}^2$ ), when the surface adsorption was saturated, were determined using the following equation:

$$A_{\min} = 10^{16} / [\square_{\max} \cdot N_{\text{av}} J]$$

$A_{\min}$  = minimum surface area in nanometer square ( $\text{nm}^2$ );  $\square_{\max}$  = maximum surface excess,  $N_{\text{av}}$  = Avogadro's number ( $6.023 \times 10^{23}$ ).

The minimum surface area depends on many factors included in the molecular structures of the surfactant<sup>[30]</sup>. Increasing of the adsorbed molecules at the interface leading to increase of the maximum surface excess values, accordingly the area available for each molecule will decrease.

### Emulsification efficiency

The emulsification process is the process which

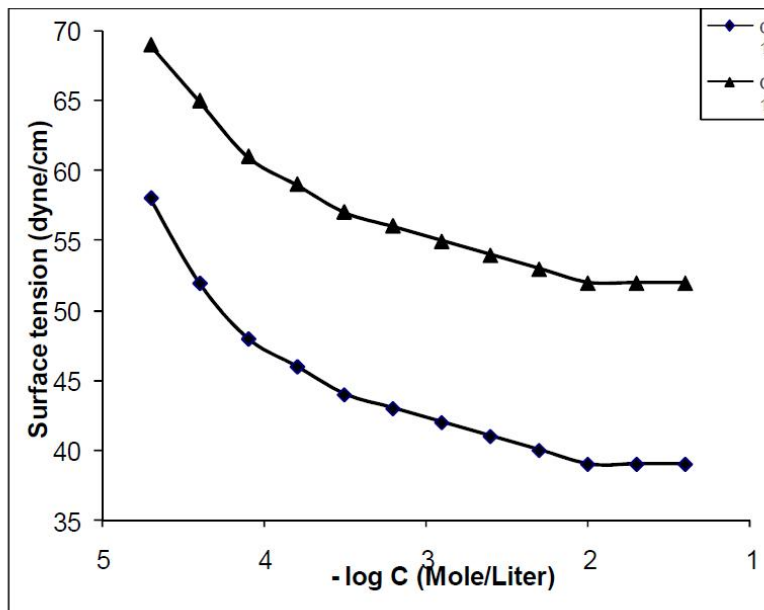


Figure 8 : Surface tension concentration profile of Q &amp; C

TABLE 2 : Surface properties of the Q and C at 25°C

Compound	CMC <sup>a</sup> (mmol/l)	$\Gamma_{cmc}^a$ (mN/m)	Pc <sub>20</sub> (mmol/l)	$\Gamma_{max} \times 10^{210}$ (molK <sup>21</sup> m <sup>21</sup> )	A <sub>min</sub> (nm <sup>2</sup> )
Q	1.4	33.7	0.039	0.73	2.27
C	1.77	35.6	6	5.55	2.99

TABLE 3 : Emulsion stability of prepared cationic surfactant compounds at 25°C

Surfactants	Emulsion stability (sec)
Q	20
C	60

enables the mixing of two immiscible phases by means of emulsifying agent. The useful emulsifiers should meet several futures including the solubility in the different phases under investigation. If yes, it will be good and efficient emulsifying agent, if not, it will be good interfacial tension reducer depending on the solubility in one phase rather than the other. The emulsification efficiency of the synthesized surfactants obtained from the emulsion stability measurements TABLE 3, showed their weak ability towards emulsification. So that, the maximum emulsion stability duration obtained was 60 seconds which is not true emulsion.

### Treatment of refinery oily wastewater

#### Treatment by using complex

The polyelectrolytes are used in removing suspended organic materials from wastewater. Since

colloidal particles are usually negatively charged, they can most readily be removed by treatment with cationic materials. Thus, cationic polyelectrolytes are the most useful of the organic polyelectrolytes. The catalytic activity of the quaternized poly vinyl pyridine with chloro silane and its complex in the cracking reaction of the crude oil could be explained by the diffusion of the polar compounds of the crude oil into the quaternized salt, and it absorb the organic pollutants and react as nuclei for cracking by the complex and chloro silane.

#### Effect of concentration of the ferric complex

The efficacy of ferric complex concentration on degradation of crude oil (5g/L) at pH 7 for 6 hours, are shown in Figure 9a. It can be observed that the degradation rate increase by increasing the concentration of the metal complex till reached to (1 g/l) then the degradation increase in slowly rate with increasing in the concentration of ferric complex as this concentration is near critical micelle concentration.

#### Effect of pH

As shown in Figure 9b, the degradation percent-

# ORIGINAL ARTICLE

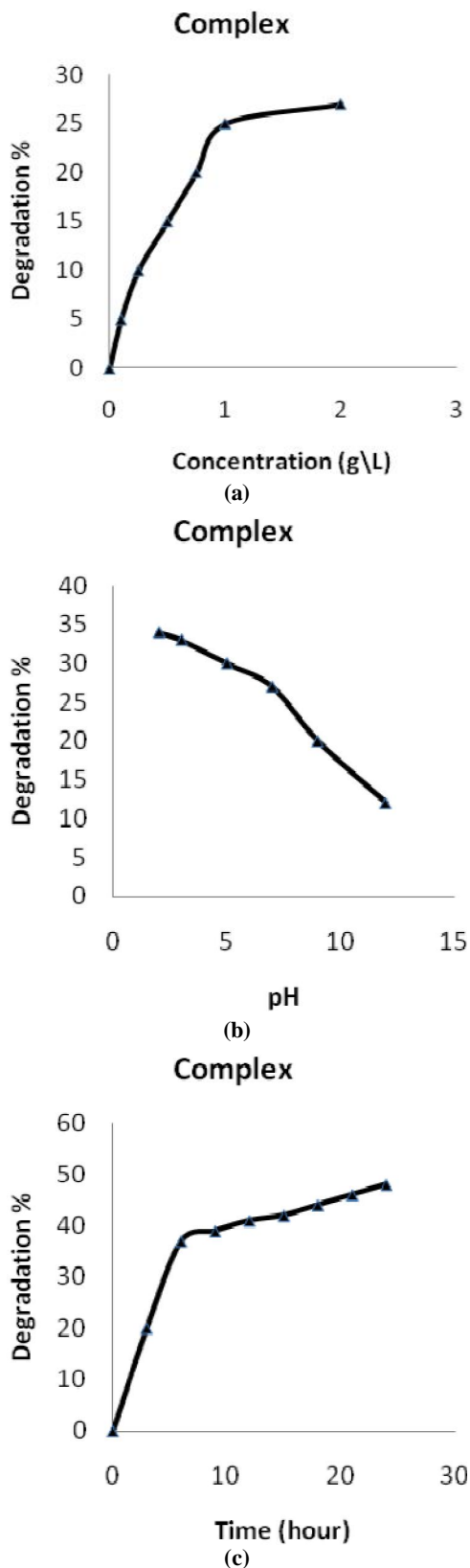


**Figure 9.** Degradation percentage of crude oil in wastewater by different concentrations of complex C at pH 7 for 6 hours (a) and by concentrations (1 g/L) of complex C at different pH for 6 hours (b) and at pH 2.5 at different times (c)

age of crude oil in wastewater (5 g/L) using concentrations (1 g/L) of complex Q at different pH for 6 hours, increase with decreasing in pH (acidic medium) and decrease with increasing in pH (basic medium). This is attributed to that acidic medium enhanced the solubility, stability and the catalytic cracking of complex.

### Effect of time

The degradation percentage of crude oil in wastewater (5 g/L) by concentration (1 g/L) of complex Q at pH 2.5 at different times increase by increasing in the time of degradation, Figure 9c.

### Treatment by fenton

#### Modified fenton reaction

Fenton oxidations have the pH optimum is reported in the acidic range near pH 3<sup>[5]</sup>. However, groundwater and soil may possess a high buffer capacity so; the necessity to acidify the reaction medium limits the applicability of the Fenton process in environmental technology. Therefore, we will evaluate the influence of quaternary salt on the rate of catalytic Fenton degradation of hydrocarbon that found in crude oil in aqueous systems at neutral pH. At this pH value, the ligand form soluble complex with iron that are able to activate H<sub>2</sub>O<sub>2</sub><sup>[31]</sup>.

#### Homogenous modified fenton reaction

#### Effect of pH value

By using the modified Fenton reaction, the catalytic systems degradation have been tested at pH values 2, 3, 5, 7 and 9 to select the best one of them. It was found that at pH 7 the optimum degradation % than others examined values, Figure 10a, due to pH-dependent behavior of catalytic systems is not clear at present since according to<sup>[32-33]</sup>, so, the stability of the complex is pH-independent in this range.

#### Effect of hydrogen peroxide concentration

The role of H<sub>2</sub>O<sub>2</sub> concentration in the catalytic degradation of wastewater taken in this investigation in the Fenton-like systems, was explained by some experiments were carried out by varying the initial H<sub>2</sub>O<sub>2</sub> concentrations at constant initial pH 7, initial complex concentration of 1 g/l for 6 hours. As shown in Figure 10b, the degradation efficiency

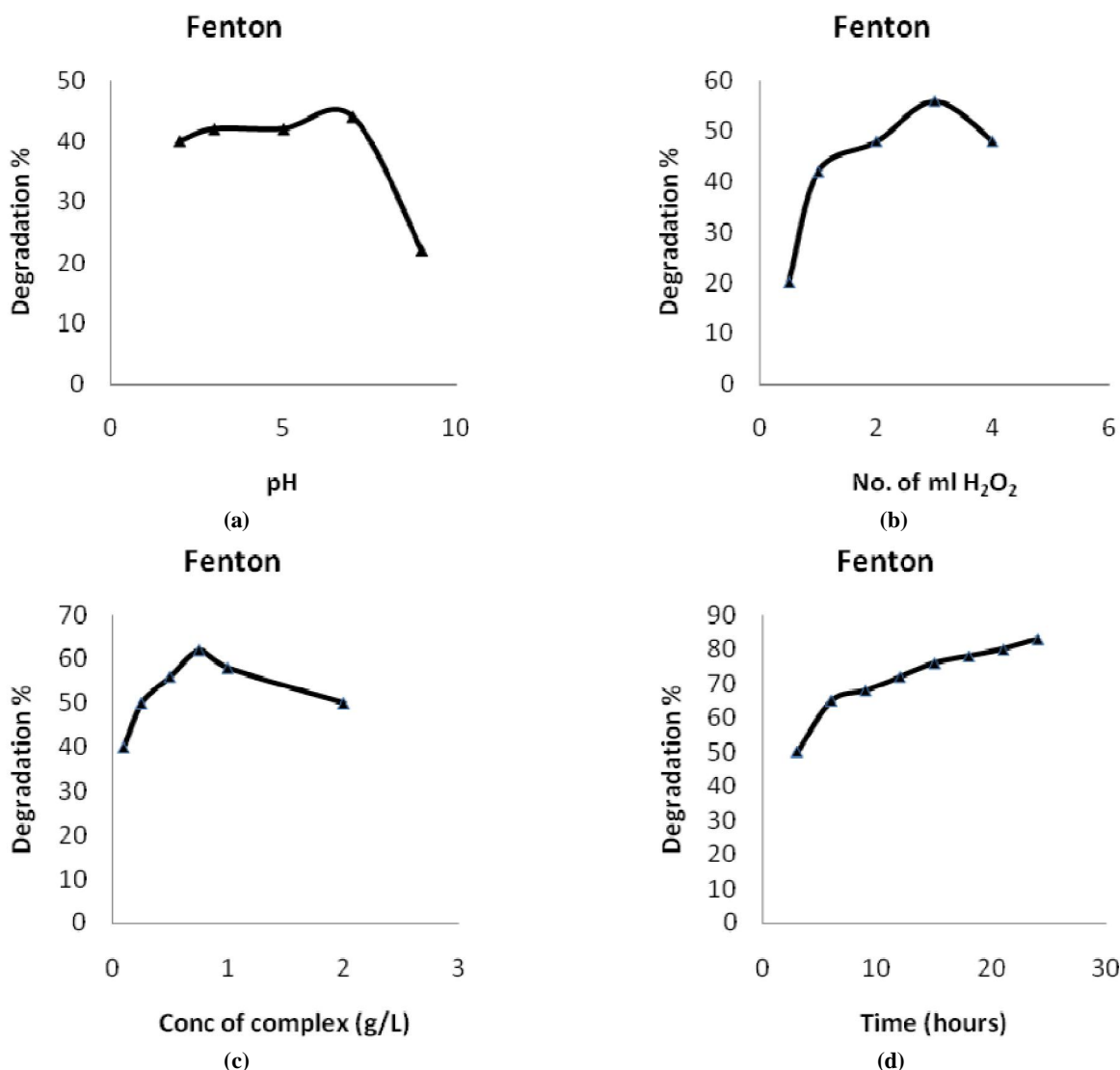
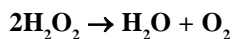


**Figure 10 : Degradation percentage of crude oil in wastewater by concentration (1 g/L) of complex C and 1ml H<sub>2</sub>O<sub>2</sub> at different pH for 6 hours (a), at pH 7 and different concentration of H<sub>2</sub>O<sub>2</sub> for 6 hours (b), by different concentrations of complex C at pH 7 in presence of 3ml H<sub>2</sub>O<sub>2</sub> for 6 hours (c) and by concentration (0.75 g/L) of complex C at pH 7 in presence of 3ml H<sub>2</sub>O<sub>2</sub> for different times(d)**

is demonstrated when H<sub>2</sub>O<sub>2</sub> concentration increases from 0 to 3 ml/L which is explained by the effect of the additionally produced .OH radical. Though, above this H<sub>2</sub>O<sub>2</sub> concentration, the reaction rate levels off and sometimes is negatively affected, by the progressive increase of the hydrogen peroxide. This may due to auto decomposition of H<sub>2</sub>O<sub>2</sub> to oxygen and water and recombination of .OH radical as the following equations:



Excess of H<sub>2</sub>O<sub>2</sub> will react with ·OH competing with organic pollutants and consequently reducing

the efficiency of the treatment, where H<sub>2</sub>O<sub>2</sub> itself contributes to the ·OH radical scavenging capacity. However, a higher dose of H<sub>2</sub>O<sub>2</sub> means a higher production of hydroxyl radicals and this dose increases because the higher H<sub>2</sub>O<sub>2</sub> concentration the more favored the occurrence of auto-scavenging reactions. Therefore, H<sub>2</sub>O<sub>2</sub> should be added at an optimal concentration (3 ml) to achieve the best degradation.

#### Effect of complex concentration

The effect of complex concentration on crude oil (5g/l) degradation was studied by conducting the experiments in presence of (0.1, 0.25, 0.5, 0.75, 1,

# ORIGINAL ARTICLE

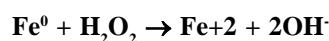
2) g/L of complex with 3 ml  $\text{H}_2\text{O}_2$ , at room temperature and pH 7 for 6 hours. It showed that the increasing in the complex concentration has a negative effect on the rate of crude oil degradation i.e. the rate decreases as the  $\text{Fe}^{3+}$  concentration increases, Figure 10c. The results of crude oil degradation via Fenton reaction, show a dependence on reaction conditions, where, the reaction between  $\text{Fe}^{2+}$  and  $\text{H}_2\text{O}_2$  produces a sufficiently  $\cdot\text{OH}$  within a short period. The lifetime of the hydroxyl radical is determined by its reactions with hydrocarbon and other present  $\cdot\text{OH}$  scavengers<sup>[34]</sup>. So, with the increase in  $[\text{Fe}^{2+}]$ , and consequently a decrease in hydrocarbon degradation rate this explains the trend shown in Figure 10c. The researchers<sup>[35]</sup> have reported that when the Fenton reaction was initiated by a high concentration of  $\text{Fe}^{2+}$  (usually more than 1mM) a sufficiently  $\cdot\text{OH}$  was produced with a short time. They indicated that under these conditions, the scavenging of  $\cdot\text{OH}$  by  $\text{Fe}^{2+}$  becomes important at high  $[\text{Fe}^{2+}] / [\text{H}_2\text{O}_2]$  ratio. Furthermore, at higher  $\text{Fe}^{2+}$  concentration, the formed  $\text{Fe}^{3+}$  could be expected to increase so that, due to very low reaction rate constant with  $\text{H}_2\text{O}_2$ , the recycling of Fenton reaction is greatly slowed down resulting in a slower rate of hydrocarbon decomposition upon increasing  $\text{Fe}^{2+}$  concentration. Generally, the latter effect appears of lower significance than the scavenging effect, unless precipitation is clearly detected<sup>[35]</sup>.

Effect of time At different times, the degradation percentage of crude oil in wastewater (5 g/L) by concentration (0.75 g/L) of complex C and 3ml  $\text{H}_2\text{O}_2$  at pH 7, increase by increasing the time of degradation, Figure 10d.

## Heterogeneous modified Fenton reaction

Fenton's oxidation, advanced oxidation catalyzed with ferrous iron  $[\text{Fe}^{2+}]$ , is successful in removing organics from water<sup>[36-37]</sup> and also soils, but required the continuous addition of dissolved  $\text{Fe}^{2+}$ . In lieu of  $\text{Fe}^{2+}$  a solid form of iron (zero-valent iron,  $\text{Fe}^0$ ) would be advantageous because it could be attached to the contaminated hydrocarbons and it could be isolated it from the solution after the reaction finished. Matheson and Tratnyek<sup>[38]</sup> investigated the application of  $\text{Fe}^0$  in permeable reactive barrier

walls instead of  $\text{Fe}^{2+}$  for dehalogenation of chlorinated organic contaminants. The equations occur in Fenton reactions are as follows;



$\text{Fe}^{2+}$  can then react with  $\text{H}_2\text{O}_2$  in traditional Fenton's oxidation reactions.



Hydroxyl radicals ( $\cdot\text{OH}$ ) generated in Fenton's reaction is the strongest oxidant leads to destruction and mineralization of organic contaminants.

## The effect of stirring time with nanocomposite CS and $\text{H}_2\text{O}_2$ on the degradation of crude oil

The experiment is performed with the optimum conditions that were used in homogenous Fenton reaction (0.75 g/l nanocomposite of CS in presence of 3ml  $\text{H}_2\text{O}_2$  at pH 7). The role of sonication was examined by the reaction was carried out in the system without ultrasound in presence of hydrogen peroxide. This experiment shows that there is very small and slow rate of the reaction where, the decomposition of 5 g/l crude oil is 37%; after 6 hour in the silent fenton and fenton type reaction with iron zero valent, Figure 11a. This indicating, that, the flow of the solution has a little effect on the decomposition rate.

## Influence of irradiation time on sonocatalytic degradation of crude oil

The application of sonolysis alone is not capable to degrade crude oil, 26% after 2h, as shown in Figure 11b. This is because it is an extremely stable contaminant that can only be destroyed by a vicious radical attack. Therefore, to reach higher removal efficiency, the combination of the oxidants and ultrasound irradiation can be applied. The controlling mechanism of sonochemical degradation of crude oil is the production of free radicals and their subsequent attack on the pollutant species. Considering this mechanism and knowing that hydrogen peroxide also dissociates in the presence of ultrasound giving hydroxyl radicals, a combination of ultrasound and hydrogen peroxide is investigated as a treatment strategy.

The sonolysis of aqueous solutions generates

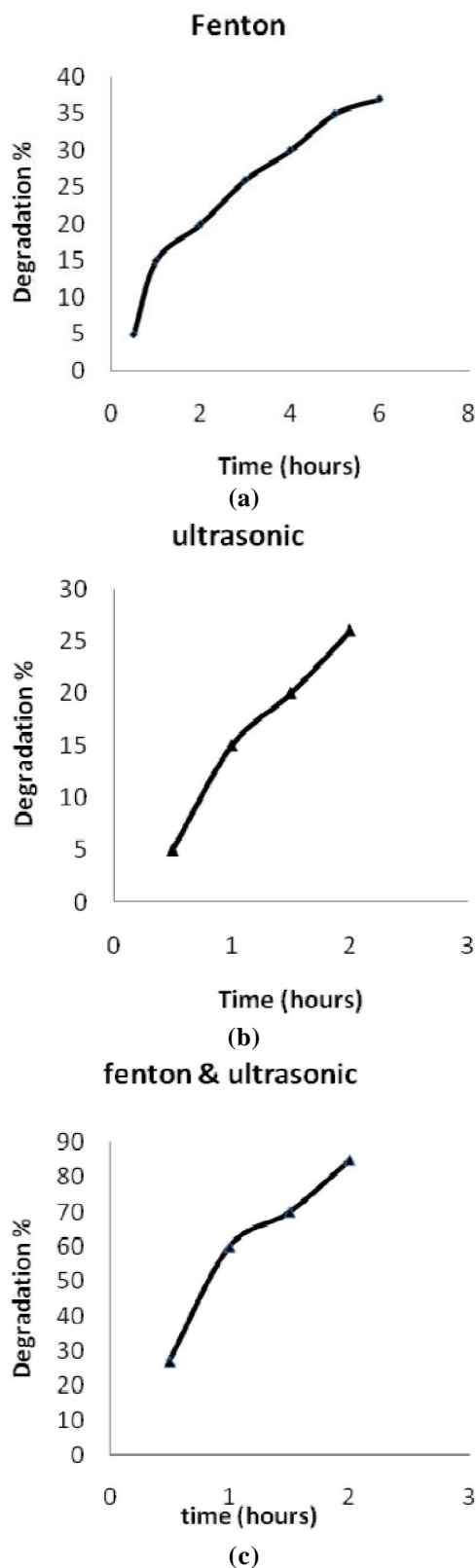


**Figure 11 :** Degradation percentage of crude oil in wastewater by initial concentration of 5 g/l, CS amounts of 0.75 g/L, 3 ml H<sub>2</sub>O<sub>2</sub> oxidant, by Influence of stirring (a), ultrasonic irradiation without CS and H<sub>2</sub>O<sub>2</sub> (b) and Fenton & ultrasonic (c) at different times with temperature of 25 °C and pH 7

highly reactive hydroxyl radical ( $\cdot\text{OH}$ )<sup>[39]</sup>. In presence of oxygen, HOO $\cdot$  radicals are formed. This leads finally to the formation of hydrogen peroxide<sup>[39]</sup>. These radicals can react with dissolved organic compounds by hydroxylation, and furthermore by oxidation in presence of air or oxygen<sup>[40]</sup>.

$\text{H}_2\text{O} + \text{H}^+ \rightarrow \cdot\text{H} + \cdot\text{OH}$  is ultrasonic

$\text{H}^+ + \text{O}_2 \rightarrow \text{HOO}\cdot$

$2\text{HOO}\cdot \rightarrow \text{H}_2\text{O}_2 + \text{O}_2$

Hydrogen peroxide will also be formed by recombination of two hydroxyl radicals<sup>[39]</sup>.

$2 \cdot\text{OH} \rightarrow \text{H}_2\text{O}_2$

Influence of irradiation time on sonocatalytic degradation of crude oil assisted with oxidant (H<sub>2</sub>O<sub>2</sub>) and heterogeneous nanocomposite

The degradation % of crude oil in the system of (Ultrasonic, H<sub>2</sub>O<sub>2</sub> and CS) with different time irradiation, reach 85% after 2 hours, Figure 11c. The application of sonolysis alone is not capable to fully degrade crude oil, because it is an extremely stable contaminant that can only be destroyed by a violent radical attack. Ultrasound irradiation provides the fragmentation of the catalyst particles with subsequent increase in the surface area, whereas the presence of solids eases the cavitation process and hence intensifies the cavitation activity in the reactor<sup>[7]</sup>. Therefore, to reach higher removal efficiency, the combination of the catalyst and ultrasound irradiation can be applied<sup>[41]</sup>, where in ultrasound the performance of the catalyst increases in view of the cavitation cleaning of the catalyst surface.

Use of ultrasound in a homogeneous system with either H<sub>2</sub>O<sub>2</sub> or fenton reagent appears to be detrimental; this emphasizes the beneficial use of ultrasound in a heterogeneous catalytic system<sup>[10]</sup>. Where, the more generation of free radical will enhance the catalytic performance in this system and by this way, process integration is conceptually advantageous in water treatment, since it can eliminate the disadvantages associated to each individual process, sonolytic and catalytic oxidation systems.

## CONCLUSIONS

These materials, quaternized salt, complex and nanocomposite of poly vinyl pyridine were pre-

# ORIGINAL ARTICLE

pared, characterized and evaluated in the degradation of crude oil in refinery petroleum wastewater (5g/L). The catalytic degradation % of the oily wastewater by these prepared materials in homogeneous and heterogeneous systems was determined by the gravimetric method. We obtained about 37% by using the systems (1 g/L of complex C at pH 2.5), and about 83% degradation of crude oil after 6 and 24 hours respectively, by using the homogeneous systems (0.75 g/L of complex C + 3 mL H<sub>2</sub>O<sub>2</sub> at pH 7). But, by using the heterogeneous systems, (0.75 g/L of nanocomposite CS + 3 mL H<sub>2</sub>O<sub>2</sub>) at pH 7, give about 39% degradation of crude oil in oily wastewater after 6 hours. In ultrasonic treatment only, the degradation % was 26% and by using the combined method, Fenton and ultrasonic irradiation (ultrasonic, 0.75 g/L of nanocomposite CS +3 mL H<sub>2</sub>O<sub>2</sub> at pH 7) was 85%. Where, in the combined method, it is observed an enhancement on the removal of hydrocarbon due to direct effect of ultrasound on the degradation of the pollutant, through increasing the surface area of the catalyst by the shock waves generated in the bulk of the solution from imploding the cavities. The shock waves also improve the mass transfer from the bulk to the surface of the catalyst.

## ACKNOWLEDGEMENT

Many thanks to all the members of petrochemicals department, and of Egypt Petroleum Research Institute (EPRI) for their valuable assistant and facilities provide.

## REFERENCES

- [1] N.Xu, W.Wang, P.Han, X.Lu; Effects of ultrasound on oily sludge deoiling, *J Hazard Mater*, **171**, 914-917 (2009).
- [2] F.Vanina, C.Delteil, Y.Padellec, V.Camel; Removal of sorbed polycyclic aromatic hydrocarbons from soil, Sludge and sediment samples using the Fenton's reagent process, *Chemosphere*, **59**, 1427-1437 (2005).
- [3] J.Yoon, Y.Lee, S.Kim; Investigation of the reaction pathway of OH radicals produced by Fenton oxidation in the conditions of wastewater treatment, *Water Sci.Technol.*, **44**(5); 15-21 (2001).
- [4] G.Lin, J.Y.Nie, N.W.Zhu, L.Wang, H.P.Yuan, Z.Shou; Enhanced Fenton's degradation of real naphthalene dye intermediate wastewater containing 6-nitro-1-diazo-2-naphthol-4-sulfonic acid: A pilot scale study, *J Chem.Eng.*, **189-190**, 108-116 (2012).
- [5] J.J.Pignatello, E.Oliveros, A.Mackay; *Crit.Rev.Env.Sci.Technol.*, **36**(1), (2006).
- [6] J.M.E.Ahad, G.F.Slater; Carbon isotope effects associated with Fenton-like degradation of toluene: potential for differentiation of abiotic and biotic degradation, *Sci.Total Environ.*, **401**, 194-98 (2008).
- [7] P.R.Gogate; *Ultrason.Sonochem.*, **15**(1) (2008).
- [8] R.Kidak, N.H.Ince; *Ultrason.Sonochem.*, **13**, 195 (2006).
- [9] A.M.T.Silva, E.Nouli, Carmo A.C.Apolinario, N.P.Xekoukoulotakis, D.Mantzavinos; *Catal.Today*, **124**, 232 (2007).
- [10] J.K.Kim, F.Martinez, I.S.Metcalf; *Catalysis Today*, **124**, 224 (2007).
- [11] A.N.Nikolopoulos, Igglessi O.Markopoulou, N.Papayannakos; *Ultrason.Sonochem.*, **13**(1), 92 (2006).
- [12] J.Liang, S.Komarov, N.Hayashi, E.Kasai; *J.Mater.Cycles Waste Manage.*, **9**, 47 (2007).
- [13] D.H.Bremner, Carlo, S.Di.; A.G.Chakinala, G.Cravotto; *Ultrason.Sonochem.*, **15**, 416 (2008).
- [14] B.Neppolian, J.S.Park, H.Choi; *Ultrason.Sonochem.*, **11**, 273 (2004).
- [15] W.X.Zhang; *J.Nanopart.Res.*, **5**, 323 (2003).
- [16] Garrido E.G.Ramírez, B.K.G.Theng, M.L.Mora; *Applied Clay Science*, **47**, 182 (2010).
- [17] N.Saleh, T.Sarbu, K.Sirk, G.V.Lowry, K.Matyjaszweski, D.Tilton; *Langmuir*, **21**(22), 9873 (2005).
- [18] W.M.Kulicke, S.Lenk, H.D.Detzner, T.Weiss; Use of polyelectrolytes in mechanical solid-solid separation, *Chem.Ing.Tech.*, **65**(5), 541 – 552 (1993).
- [19] C.E.Reineke, J.A.Jagodzinski, K.R.Denslow; Highly water selective cellulosic polyelectrolyte membranes for the pervaporation of alcohol water mixtures, *J.Membr.Sci.*, **32**(2 – 3), 207 – 221 (1987).
- [20] C.Chovino, P.Gramain; Influence of the conformation on chemical modification of polymers: Study of the quaternization of poly (4-vinylpyridine). *Macromolecules*, **31**(20), 7111 – 7114 (1998).
- [21] H.Dautzenberg, W.Jaeger, J.Kotz, B.Philipp, C.H.Seidel, D.Stscherbina; Synthesis of polyelectrolytes, *Polyelectrolytes*; Hanser/Gardner Publica-

- tions Inc., Cincinnati, 9 – 86 (1994).
- [22] A.M.Al-Sabagh, A.F.El-Kafrawy, T.T.Khidr, R.A.El-Ghazawy, M.R.Mishrif; *J.of Dispersion Science and Technology*, **28**, 976 (2007).
- [23] D.Eley, M.J.Hey, D.Symonds; *Colloids and Surfaces A*, **32**, 87 (1988).
- [24] ASTM F2259.
- [25] Y.Sun, X.Li, J.Cao, W.Zhang, H.P.Wang; *Advances in Colloid and Interface Science*, **47**, 120 (2006).
- [26] Y.Liu, S.A.Majetich, R.D.Tilton, D.S.Sholl, G.V.Lowry; *J.Environmental Science & Technology*, **39**, 1338 (2005).
- [27] C.Wang, W.Zhang; *J.Environmental Science & Technology*, **31**, 2154 (1997).
- [28] B.Q.Zhang, Y.X.Hua; *Electrochimica Acta*, **54**, 1881 (2009).
- [29] M.Shuichi, I.Kazayasu, Y.Sadao, K.Kazuo, Y.Tsuyoshi; *J.Am.Oil Chem.Soc.*, **67**, 996 (1991).
- [30] S.M.Hamid, D.C.Sherrington; *Brit.Polymer J.*, **16**, 39 (1984).
- [31] A.Georgi, A.Schierz, U.Trammler, C.P.Horwitz, T.J.Collins, F.D.Kopinke; *Appl.Catal.B: Environmental*, **72**, 26 (2007).
- [32] M.G.Park, M.H.Choi; United state patent application publication No: US/0128799 A1, (2006).
- [33] M.G.Park, M.H.Choi; United state patent application publication No: US/7375243, (2008).
- [34] G.V.Buxton, C.L.Greenstock, W.P.Helman, A.B.Ross; *J.Phys.Chem.Ref.Data*, **17**(2), 513 (1988).
- [35] J.Yoon, Y.Lee, S.Kim; *Water Sci.Technol.*, **44**, 15 (2001).
- [36] J.Bergendahl, S.Hubbard, D.Grasso; *J.Haz.Mat.*, **99**, 43 (2003).
- [37] G.Chen, G.E.Hoag, P.Chedda, F.Nadim, B.A.Woody, G.M.Dobbs; *J.Haz.Mat.*, **87**, 171 (2001).
- [38] L.J.Matheson, P.G.Tratnyek; *Environ.Sci.Technol.*, **28**(12), 2045 (1994).
- [39] E.J.Hart, A.Henglein; *J.Phys.Chem.*, **89**, 4342 (1985).
- [40] A.Tauber, H.P.Schuchmann, C.V.Sonntag; *J.Chem.Soc.Perkin Trans.*, **2**, 1129 (1999).
- [41] E.Psillakis, G.Goula, N.Kalogerakis, D.Mantzavinos; *J.Hazard.Mat.*, **108**, 95 (2004).